BUTTERWORTH HEINEMANN

Fully developed flow and heat transfer in semi-elliptical ducts

K. Velusamy
Thermal Hydaulics Section, Indira Gandhi Centre for Atomic Research, Kalpakkam, India
Vijay K. Garg
Internal Fluid Mechanics Division, NASA Lewis Research Center, Cleveland, OH, USA
G. Vaidyanathan
Thermal Hydraulics Section, Indira Gandhi Centre for Atomic Research, Kalpakkam, India

A control volume-based numerical solution is described for the fully developed laminar flow and heat transfer in ducts of semi-elliptical cross section. Both an isothermal and a uniform axial heat flux condition on the duct walls have been considered. Numerical results for velocity and temperature profiles, friction factor, pressure defect, and Nusselt number are presented for a wide range of duct aspect ratios from 0.1 to 0.999. Comparison with earlier numerical results for the limiting case of semicircular duct and with analytical solution for fully elliptical ducts is excellent. For ducts in which the baseplate is on the major axis, friction factor and Nusselt number for the uniform heat flux condition increase as the aspect ratio decreases, with values for the lowest aspect ratio of 0.1 being about 25 percent larger than those for a semicircular duct. For ducts with the baseplate on the minor axis, all characteristics exhibit a nonmonotonic behavior with respect to the aspect ratio. While the maximum velocity and pressure defect exhibit a mild maximum for aspect ratio of 0.6, the friction factor and Nusselt number exhibit a minimum at the same aspect ratio. The ratio of Nusselt number to friction factor is higher for semi-elliptical ducts in comparison to that for other ducts, such as sinusoidal, circular segmental, and isosceles triangular ducts.

Keywords: laminar flow and heat transfer; semi-elliptical ducts; control volume analysis

Introduction

Ducts having noncircular cross sections are used extensively today in refrigeration and air-conditioning applications. Ducts having an elliptical cross section are occasionally used in compact heat exchangers where moderate increase in heat transfer is required. Elliptical ducts also assume importance as the pressure drop encountered by the fluid flowing over such ducts is less than that over circular ducts. A semi-elliptic duct has a flat base and a curved wall of elliptic shape. The flat base can be conveniently used to wind a tube of semi-elliptic cross section over any box-type structure, such as a deep freezer in a refrigerator. The semi-elliptic ducts also serve as a lower bound of internally finned elliptic ducts. Moreover, a semicircular duct can assume a nearly semi-elliptic shape attributable to either manufacturing tolerance or deformation during service. Ducts of semicircular cross section have been analyzed extensively by Hong and Bergles (1976), Shah and London (1978), Manglik and Bergles (1988), Lei and Trupp (1989a, b; 1990), and Ben-Ali et al. (1989). Fully elliptical ducts have been analyzed by Bhatti (1983, 1984), Abdel-Wahed et al. (1984), Ebadian et al. (1986), Garg and Velusamy (1989), Dong and Ebadian (1991, 1992a, b), and Velusamy and Garg (1993).

Address reprint requests to Dr. V. K. Garg, Internal Fluid Mechanics Div., NASA Lewis Research Center, Mail Stop 5-11, Cleveland, OH 44135.

Received 28 March 1994; accepted 4 November 1994

Int. J. Heat and Fluid Flow 16: 145–152, 1995

655 Avenue of the Americas, New York, NY 10010

Laminar flow development in the entrance region of elliptic ducts is described by Bhatti (1983), Abdel-Wahed et al. (1984), Garg and Velusamy (1989), and by Velusamy and Garg (1993). Fully developed heat transfer in elliptical ducts is discussed by Bhatti (1984), and Ebadian et al. (1986). Dong and Ebadian (1991, 1992a) deal with flow and temperature characteristics in curved elliptical ducts, while Dong and Ebadian (1992b) deal with the interaction of radiation and convection in the entrance region of elliptical ducts with internal fins. It seems that the problem of fully developed flow and heat transfer in semi-elliptical ducts has not been given any attention (cf. Eckert et al. 1992, and similar earlier reviews) except by Shah and Bhatti (1987).

The analysis of Shah and Bhatti (1987) is quite preliminary. They presented an analytical expression for friction factor in semi-elliptical ducts, employing a graphical method also known as the 3R method. The analytical expression is in error, however, because the product of friction factor and Reynolds number given by the expression is 5.012 for a semicircular duct as against the actual value of 15.767. Also, Shah and Bhatti did not analyze other characteristics such as pressure defect, Nusselt number, etc.

Herein, we analyze fully developed laminar flow and heat transfer characteristics in semi-elliptical ducts. We present results for two types of ducts, one with the baseplate on the major axis (Figure 1a) and another with baseplate on the minor axis (Figure 1b). Two types of thermal boundary conditions; namely, an isothermal wall (the (T) condition), and a uniform axial heat rate per unit of duct length with circumferentially

SSDI 0142-727X/95/$10.00
SSDI 0142-727X(94)00019-9

uniform wall temperature (the Ⓗ condition) have been considered for both the ducts.

Analysis

Consider an incompressible, Newtonian fluid flowing through a straight duct of semi-elliptical cross section. We assume negligible body forces and fully developed laminar flow with constant properties. We use elliptic cylinder coordinates (ξ, η, z), as shown in Figure 1c. This coordinate system consists of an orthogonal family of confocal ellipses and hyperbolas in a plane, translated in the third (axial here) direction normal to the plane. The surfaces η = constant are the confocal elliptic cylinders, while the surfaces ξ = constant are the hyperbolic cylinders, given by the following:

$$\frac{x^2}{(c\cosh\eta)^2} + \frac{y^2}{(c\sinh\eta)^2} = 1$$

$$\frac{x^2}{(c\cos\xi)^2} - \frac{y^2}{(c\sin\xi)^2} = 1$$

The normalized equations for conservation of momentum, mass, and energy are:

Axial momentum:

$$\frac{1}{H^2}\left[\frac{\partial^2 W}{\partial\xi^2} + \frac{\partial^2 W}{\partial\eta^2}\right] = \frac{dP}{dZ} \tag{1}$$

Integral continuity:

$$\int_{\xi=0}^{\pi/2}\int_{\eta=0}^{\eta_w} WH^2\, d\xi\, d\eta = \frac{\pi}{4}\frac{ab}{D_h^2} \tag{2}$$

Energy equation for the Ⓣ *condition*:

$$\frac{1}{H^2}\left[\frac{\partial^2\Phi}{\partial\xi^2} + \frac{\partial^2\Phi}{\partial\eta^2}\right] = 4W\frac{\Phi}{\Phi_m} \tag{3}$$

Energy equation for the Ⓗ *condition*:

$$\frac{1}{H^2}\left[\frac{\partial^2\Phi}{\partial\xi^2} + \frac{\partial^2\Phi}{\partial\eta^2}\right] = 4W \tag{4}$$

where

$$\Phi_m\left(\frac{\pi}{4}\frac{ab}{D_h^2}\right) = \int_{\xi=0}^{\pi/2}\int_{\eta=0}^{\eta_w} W\Phi H^2\, d\xi\, d\eta \tag{5}$$

Equations 1, 3, and 4 are subject to the following boundary conditions.

Case 1 Baseplate on the major axis:

$$\begin{aligned} &W = 0 = \Phi \quad \text{along} \quad \eta = 0, \eta_w \quad \text{for all} \quad \xi \\ &W = 0 = \Phi \quad \text{along} \quad \xi = 0 \quad \text{for all} \quad \eta \\ &\partial W/\partial\xi = 0 = \partial\Phi/\partial\xi \quad \text{along} \quad \xi = \pi/2 \quad \text{for all} \quad \eta \end{aligned} \tag{6a}$$

Notation

a	semimajor axis of the elliptical section
b	semiminor axis of the elliptical section
B	width of the baseplate
Bi	Biot number ($= \bar{h}D_h/k_w$)
c	focal distance of the elliptical section
C_p	specific heat of the fluid
d	thickness of the duct wall
D_h	hydraulic diameter of the semi-elliptical section
$E(m)$	complete elliptic integral of second kind
f	friction factor
$\bar{h}$	circumferentially averaged heat transfer coefficient
H	$(c/D_h)(\sinh^2\eta + \sin^2\xi)^{1/2}$
k	thermal conductivity of the fluid
k_w	thermal conductivity of the wall material
$K(\infty)$	pressure defect
L	height of the duct cross section relative to the baseplate
m	$= (1 - \lambda^2)^{1/2}$
Nu_H	average Nusselt number for uniform axial heat flux condition
Nu_T	average Nusselt number for the isothermal wall condition
n_ψ	number of control volumes in the cross section for the variable ψ
p	dimensional pressure
P	dimensionless pressure $[= p/(\rho\bar{w}^2)]$
$\bar{q}''$	average heat flux on the duct wall $[= (1/4)(\rho C_p\bar{w}D_h)\, dt_m/dz]$
$r_{i\psi}$	residue of the discretized equation for ith control volume for the variable ψ
Re	Reynolds number $(= \bar{w}D_h/\nu)$
R_ψ	absolute sum of $r_{i\psi}$ taken over n_ψ
t	temperature of the fluid
t_m	mean temperature of the fluid
t_w	temperature of the duct wall
w	axial velocity in the duct
$\bar{w}$	average axial velocity in the duct
W	dimensionless counterpart of $w(= w/\bar{w})$
x	cross stream Cartesian coordinate (Figure 1)
X	$= x/a$
y	cross stream Cartesian coordinate (Figure 1)
z	axial coordinate (along the flow direction)
Z	dimensionless axial coordinate $[= z/(D_h\mathrm{Re})]$

Greek

ε	a small number for checking convergence
η	elliptic cylinder coordinate (Figure 1)
η_w	value of η at the curved wall
λ	aspect ratio of the duct $(= b/a)$
ν	kinematic viscosity of the fluid
ξ	elliptic cylinder coordinate (Figure 1)
ρ	density of the fluid
θ	$= (\Phi - \Phi_c)\pi/E(m)$
Φ	dimensionless temperature of fluid $[= (t - t_w)k/(\bar{q}''D_h)]$
$(\Delta t)_c$	circumferential temperature difference in the duct wall
Φ_c	value of Φ at duct axis for fully elliptic duct
Φ_m	dimensionless mean temperature of fluid, Equation 5

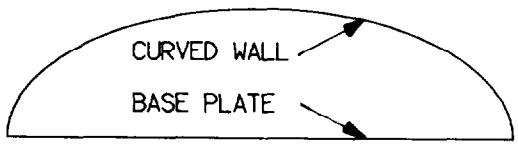

Fig. 1a

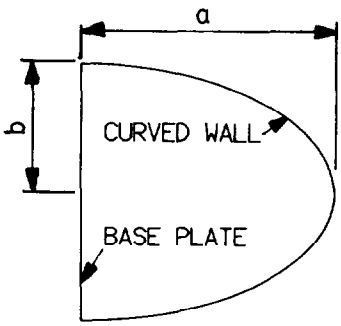

Fig. 1b

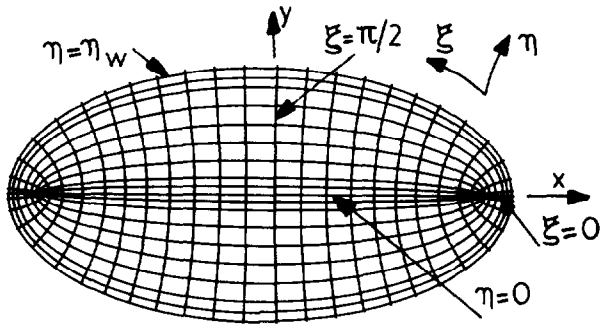

Fig. 1c

Figure 1 (*a*) Duct with baseplate on major axis; (*b*) Duct with baseplate on minor axis; and (*c*) Elliptic-cylinder coordinate system

Case 2 Baseplate on the minor axis:

$$W = 0 = \Phi \quad \text{along} \quad \eta = \eta_w \quad \text{for all} \quad \xi$$
$$W = 0 = \Phi \quad \text{along} \quad \xi = \pi/2 \quad \text{for all} \quad \eta$$
$$\partial W/\partial \xi = 0 = \partial \Phi/\partial \xi \quad \text{along} \quad \xi = 0 \quad \text{for all} \quad \eta$$
$$\partial W/\partial \eta = 0 = \partial \Phi/\partial \eta \quad \text{along} \quad \eta = 0 \quad \text{for all} \quad \xi \tag{6b}$$

In Equations 2 and 5, the hydraulic diameter D_h is given by the following: $D_h = \pi b/(E(m) + 1)$ for baseplate along the major axis; and $D_h = \pi b/(E(m) + \lambda)$ for baseplate along the minor axis.

From first principles and definitions given in the Nomenclature, the product of friction factor and Reynolds number is $f\mathrm{Re} = (1/2)\, dP/dZ$, and the Nusselt number is Nu_T or $\mathrm{Nu}_H = \bar{h}D_h/k = -1/\Phi_m$. The pressure defect, due to flow development, via the method of Lundgren et al. (1964) is

$$K(\infty) = \frac{8D_h^2}{\pi ab} \int_{\xi=0}^{\pi/2} \int_{\eta=0}^{\eta_w} (W - 1)W^2H^2 \, d\xi \, d\eta$$

The boundary condition of Ⓣ type occurs in such heat exchangers as evaporators and condensers; whereas, the boundary condition of Ⓗ type occurs in such applications as radiant heating, electric resistance heating, and in counterflow heat exchangers when the fluid capacity rates are the same. By comparing the heat transfer within the duct wall in the circumferential direction to the heat transfer from the wall to the fluid. it can be shown that $(\Delta t)_c/(t_w - t_m) = BiD_h/d$. Thus, the Ⓗ-type boundary condition is also applicable for cases having $\mathrm{Bi}D_h/d \ll 1$; that is, in the case of thick duct walls made up of a highly conducting material with small hydraulic diameter and relatively low heat transfer coefficient to the fluid.

Solution

Equations 1–6 are solved by the control volume-based discretization method (Patankar, 1980). To evaluate the axial pressure gradient in the duct via the integral continuity Equation 2, the method proposed by Raithby and Schneider (1979) is used. Once the axial velocity is obtained from Equations 1 and 2, Equations 3 and 5 are solved iteratively for the Ⓣ boundary condition, and Equation 4 is solved for the Ⓗ condition in order to get the temperature distribution. The discretization procedure yields a set of algebraic equations for each variable. The pentadiagonal system of algebraic equations for each variable is solved by a plane-by-plane method (Velusamy) 1989). This method is an extension of the Thomas algorithm for the tridiagonal system of equations. Convergence is assumed once the absolute sum of the residue R_ψ corresponding to the variable ψ in the discretization equation is less than ε where

$$R_\psi = \sum_{i=1}^{n_\psi} |r_{i\psi}|$$

The value of ε is taken to be 10^{-6} for the results presented herein.

In the cross-stream ($\xi - \eta$) plane a 52 × 52 nonuniform grid pattern was used except for the semicircular duct, considered here as a semi-elliptical duct with aspect ratio 0.999, for which only a 40 × 40 grid pattern was employed. Grids were packed near the duct wall where large velocity gradients persist. For some cases, a 27 × 27 grid pattern with double the grid size was also tried. The maximum deviation between the results of fine and coarse grid patterns was only 0.2 percent. Moreover, the present results for the semicircular duct match almost exactly with the results reported in literature. These studies confirm that the grid size selected (52 × 52) is satisfactory.

Accuracy

To validate the computer program, the well-studied problem of flow in a semicircular duct was computed first. The aspect ratio for this study was taken to be 0.999 because the coordinate transformation is singular for $\lambda = 1$. The present values of maximum velocity in the duct, friction factor, pressure defect, and Nusselt number are shown in Table 1 along with those of Lei and Trupp (1989a), Ben-Ali et al. (1989), and Shah and London (1978). Clearly, the present values match almost exactly the literature values.

Table 1 Fully developed flow in semi-elliptical ducts

	Present values for $\lambda = 0.999$	Literature values for $\lambda = 1$
W_{max}	2.0605	2.0613*
$2\,f\mathrm{Re}$	31.531	31.534†
$K(\infty)$	1.466	1.463†
Nu_T	3.318	3.316‡
Nu_H	4.082	4.089†

* Lei and Trupp (1989a)
† Shah and London (1978, 265)
‡ Ben-Ali et al. (1989)

Table 2 W and θ along the major axis of a fully elliptic duct ($\lambda = 0.1$)

	W		$\theta = (\Phi - \Phi_c)\pi/E(m)$	
X	Present	Equation (7)	Present	Equation (8)
1.0	0.0	0.0	1.0586	1.0581
0.9002	0.3791	0.3792	1.0143	1.0150
0.7860	0.7641	0.7643	0.8943	0.8950
0.7074	0.9989	0.9993	0.7841	0.7848
0.5908	1.3010	1.3018	0.6006	0.6013
0.5165	1.4660	1.4665	0.4813	0.4819
0.3836	1.7050	1.7057	0.2834	0.2837
0.2995	1.8200	1.8205	0.1779	0.1782
0.0952	1.9810	1.9819	0.0183	0.0187
0.0	1.9990	2.0	0.0	0.0

As another validation of the numerical procedure, the problem of flow through a fully elliptic duct with an aspect ratio of 0.1 was solved by replacing the baseplate with symmetry boundary conditions. The predicted values of $f\mathrm{Re}$ and Nu_H are 19.307 and 5.125 against the analytical values (Shah and Bhatti 1987) of 19.314 and 5.124, respectively. Along the major axis, the analytical expressions for the velocity (Shah and Bhatti) and temperature profiles (Bhatti 1984) corresponding to the Ⓗ boundary condition in a fully elliptic duct are

$$W = 2(1 - X^2) \tag{7}$$

$$\theta = \frac{2E(m)}{3\pi(1+\lambda^2)(1+6\lambda^2+\lambda^4)}\{(5+\lambda^2)X^2[2(3\lambda^2+1) - (1+\lambda^2)X^2]\} \tag{8}$$

where $\theta = (\Phi - \Phi_c)\pi/E(m)$ and Φ_c is the temperature at the duct centerline. In Table 2, the present numerical results are compared against the analytical values from Equations 7 and 8 for $\lambda = 0.1$. The comparison is excellent.

Results and discussion

Results were obtained for aspect ratio λ varying from 0.1 to 0.999 for both ducts and for both thermal conditions on the duct wall. The velocity and temperature distribution along the minor axis of a semi-elliptical duct with baseplate along the major axis are shown in Figures 2, 4 and 5. The corresponding results along the major axis of a semi-elliptical duct with baseplate along the minor axis are shown in Figures 6, 8 and 9. Results for the maximum velocity in the duct, friction factor, pressure defect, and Nusselt number are shown in Figures 3 and 7, respectively, for the ducts with baseplate along the major axis, and that along the minor axis.

Semi-elliptical duct with baseplate on the major axis

Figure 2 compares the axial velocity distribution along the minor axis for $\lambda = 0.1$ and 0.999. Clearly, the velocity distribution is similar in both cases, with the location of maximum velocity moving toward the center of the duct ($y/b = 0.5$) as the aspect ratio decreases. For example, the maximum velocity occurs at $y/b = 0.467$ for $\lambda = 0.999$, and at $y/b = 0.498$ for $\lambda = 0.1$. This is caused by the increasing participation of baseplate in shearing the fluid as the aspect ratio decreases. Also shown in Figure 2 is the axial velocity profile reported by Manglik and Bergles (1988) for a semicircular duct. Clearly, the present results for $\lambda = 0.999$ match almost exactly with those of Manglik and Bergles, indicating the validity of the present results.

From Figure 3 we find that the value of maximum velocity decreases, but slightly, with decreasing aspect ratio. It may be pointed out that the value of maximum velocity for semi-elliptical ducts is nowhere near that for parallel plate ducts, even for aspect ratio of 0.1. The pressure defect caused by entrance flow $K(\infty)$ decreases with the aspect ratio. A reason for this reduction is that the gain in momentum of the fluid in small aspect ratio ducts is less than that in large aspect ratio ducts. This is evident from the disparity in the value of maximum velocity.

Figure 4 compares the temperature distribution along the minor axis for $\lambda = 0.1$ and 0.999, for the Ⓗ boundary condition on the duct walls. Clearly, the temperature profiles in the two cases are also similar, with the location of maximum

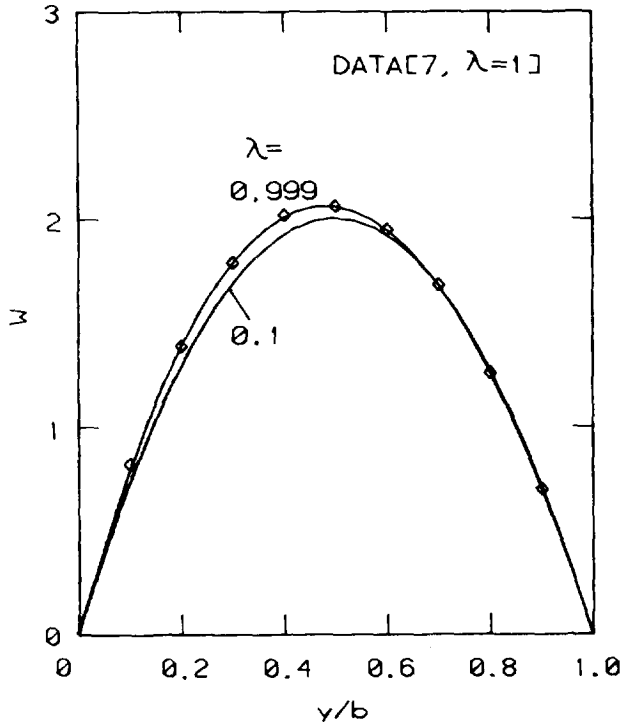

Figure 2 Axial velocity along the minor axis of a duct with baseplate on the major axis

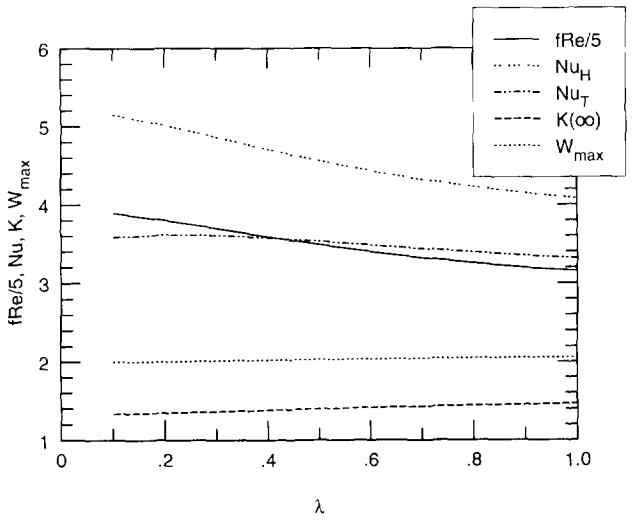

Figure 3 Variation of various quantities with the aspect ratio for ducts with baseplate on the major axis

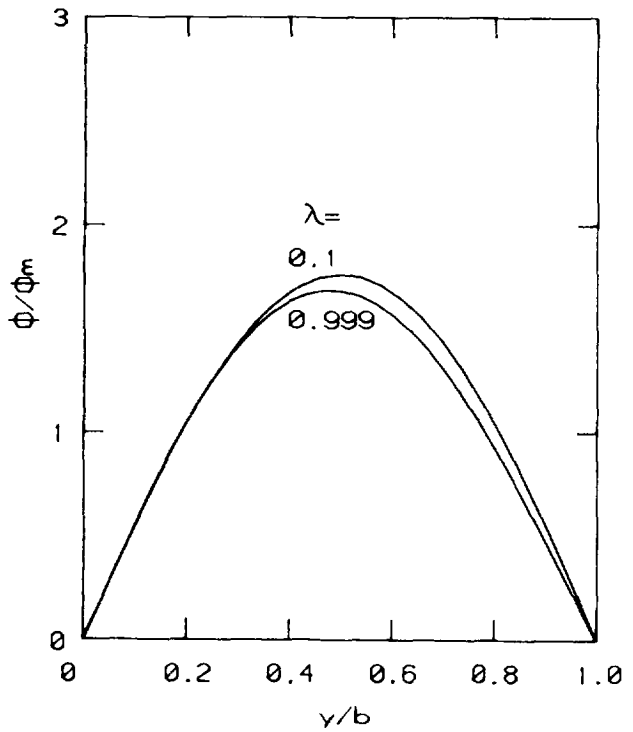

Figure 4 Temperature along the minor axis of a duct with baseplate on the major axis for the (H) boundary condition

value moving toward the center of the duct as the aspect ratio decreases. The friction factor and fully developed Nusselt number for the (H) boundary condition are shown in Figure 3. It is clear that both the friction factor and Nu_H increase as the aspect ratio decreases; both values for $\lambda = 0.1$ being about 25 percent more than those for the semicircular duct. A reason for this increase is the increased surface area associated with low aspect ratio ducts. Values of $f\mathrm{Re}$ and Nu_H for $\lambda = 0.1$ are 19.458 and 4.636, respectively, against the parallel plate duct values of 24.0 and 8.235. The lower values in the case of semi-elliptic ducts are caused by the nonuniform flow distribution.

For the (T) boundary condition, Figure 5 compares the temperature distribution along the minor axis for various values of the aspect ratio. Clearly, the maximum value of Φ/Φ_m increases considerably as the aspect ratio decreases; the ratio of maximum value for $\lambda = 0.1$ to that for a semicircular duct being ~ 2.25. Figure 5 also compares the present results for a semicircular duct with those of Manglik and Bergles (1988). The comparison is again excellent. Nusselt number values for the (T) boundary condition, also shown in Figure 3, show a maximum near $\lambda = 0.2$. However, the difference between Nu_T values for $\lambda = 0.2$ and for the semicircular duct is only ~ 9 percent.

Comparison with other ducts. Let L be the height of the duct cross section and B the base width. Hence, for a semi-elliptic duct with base on the major axis, $L/B = \lambda/2$. For the purpose of comparing the true heat transfer effectiveness of the ducts, two more parameters $F_T = Nu_T/(2f\mathrm{Re})$ and $F_H = Nu_H/(2f\mathrm{Re})$ are defined. Under identical values of L/B, a semi-elliptic duct with base on the major axis resembles sinusoidal, isosceles triangular, and circular segmental ducts. Table 3 provides a comparison amongst these configurations in terms of values of $f\mathrm{Re}$, Nu_T, Nu_H, F_T, and F_H for three typical values of L/B. It can be seen that as L/B decreases, $f\mathrm{Re}$, Nu_T, and Nu_H decrease monotonically for all duct configurations except the semi-elliptic one, for which they increase monotonically as the duct gets compressed. The values of F_T and F_H are higher for the semi-elliptic duct compared to the other ducts. Also, as L/B decreases, the value of F_H increases for the semi-elliptic duct, while the reverse is true for the other geometries. These facts exhibit the superiority of semi-elliptic ducts over other ducts compared herein.

Semi-elliptic duct with baseplate on the minor axis

Figure 6 compares the axial velocity distribution along the major axis for various values of λ for the duct with baseplate on the minor axis. It can be seen from this figure that the location of maximum velocity moves toward the baseplate as the aspect ratio decreases. This is caused by increased shear offered by the curved wall of the duct as the aspect ratio decreases. This is contrary to the behavior exhibited by the velocity profiles in Figure 2 for ducts with baseplate on the major axis. The values of maximum velocity, friction factor, and pressure defect for this duct are shown in Figure 7 as a function of the aspect ratio. From this figure, we find that these

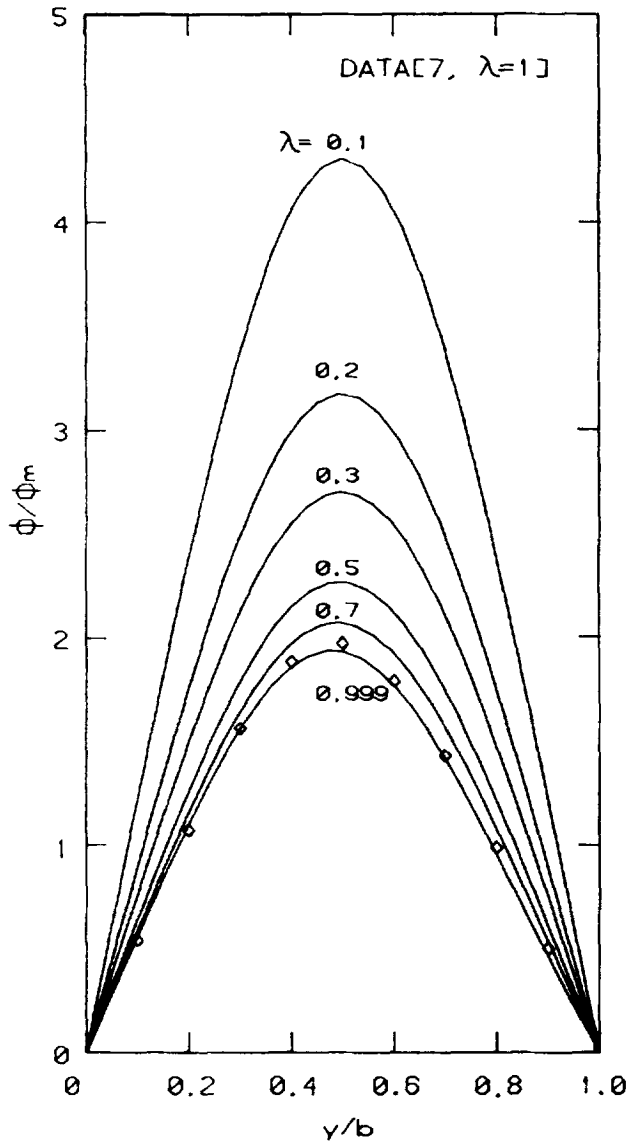

Figure 5 Temperature along the minor axis of a duct with baseplate on the major axis for the (T) boundary condition

Table 3 Comparison of results for semi-elliptic duct with base on the major axis with those for other ducts

	L/B	λ	Semi-elliptic duct*	Sinusoidal duct†	Isosceles triangular duct†	Circular segmental duct†
	0.5	1.0	31.531	22.414	26.306	31.534
2 *f* Re	0.25	0.5	34.876	20.246	25.244	31.340
	0.125	0.25	37.467	19.486	24.392	31.186
	0.5	1.0	3.318	2.12	2.34	—
Nu_T	0.25	0.5	3.533	1.80	1.90	—
	0.125	0.25	3.612	—	1.47	—
	0.5	1.0	4.082	2.617	2.982	4.089
Nu_H	0.25	0.5	4.562	2.213	2.603	3.846
	0.125	0.25	4.939	2.017	2.302	3.687
	0.5	1.0	0.1052	0.0946	0.0889	—
F_T	0.25	0.5	0.1013	0.0889	0.0753	—
	0.125	0.25	0.0964	—	0.0603	—
	0.5	1.0	0.1295	0.1168	0.1134	0.1297
F_H	0.25	0.5	0.1308	0.1093	0.1031	0.1227
	0.125	0.25	0.1318	0.1035	0.0944	0.1182

* with base on the major axis
† Shah and London (1978)

values show a nonmonotonic behavior with respect to λ. While the maximum velocity and pressure defect exhibit a mild maximum near $\lambda = 0.6$, the friction factor passes through a minimum at $\lambda = 0.6$. Reasons for such a behavior are similar to those given above.

For the Ⓗ boundary condition, Figure 8 compares the temperature distribution along the major axis for various values of the aspect ratio. It can be observed from this figure that the maximum value of Φ/Φ_m passes through a minimum at $\lambda = 0.5$. Also, as the aspect ratio decreases, the location of maximum temperature moves toward the baseplate. This is contrary to the behavior observed in Figure 4 for ducts with baseplate on the major axis. Variation of Nu_H with λ is shown in Figure 7. Clearly, Nu_H passes through a minimum at $\lambda = 0.6$.

For the Ⓣ boundary condition, Figure 9 shows the temperature profiles along the major axis for various values of λ. It is observed from this figure that the maximum value of Φ/Φ_m exhibits a minimum with respect to the aspect ratio. The maximum value of Φ/Φ_m for $\lambda = 0.1$ is about 1.4 times that for a semicircular duct. Also, the location of the maximum temperature moves toward the baseplate as λ decreases. Another observation worth noting is that for a considerable length around the focal point, the fluid temperature along the major axis is nearly equal to the wall temperature, especially for low-aspect ratio ducts. Variation of Nu_T with λ is shown in Figure 7. Just as with Nu_H, Nu_T also exhibits a minimum near $\lambda = 0.6$, but the magnitude of variation is smaller.

Comparison with other ducts. For the semi-elliptic duct with base on the minor axis, $L/B = 0.5/\lambda$. Table 4 compares the values of fRe, Nu_T, Nu_H, F_T, and F_H for such a semi-elliptic

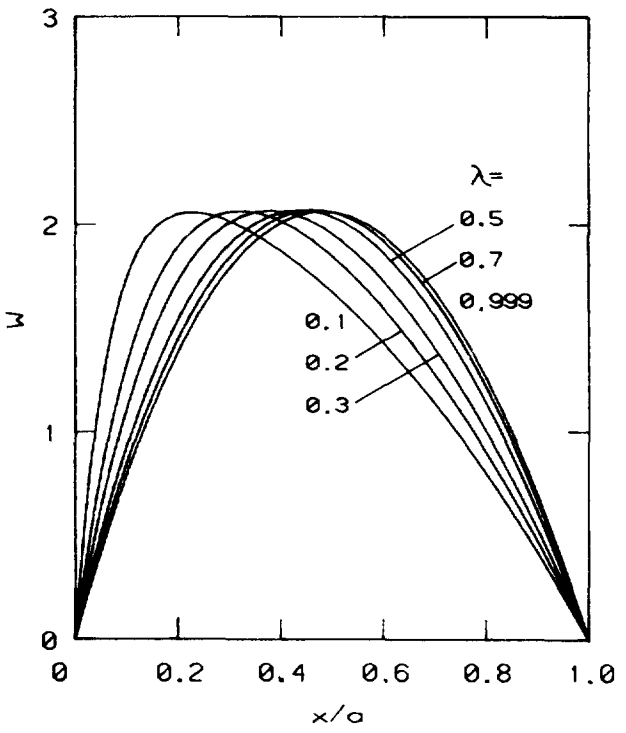

Figure 6 Axial velocity along the major axis of a duct with baseplate on the minor axis

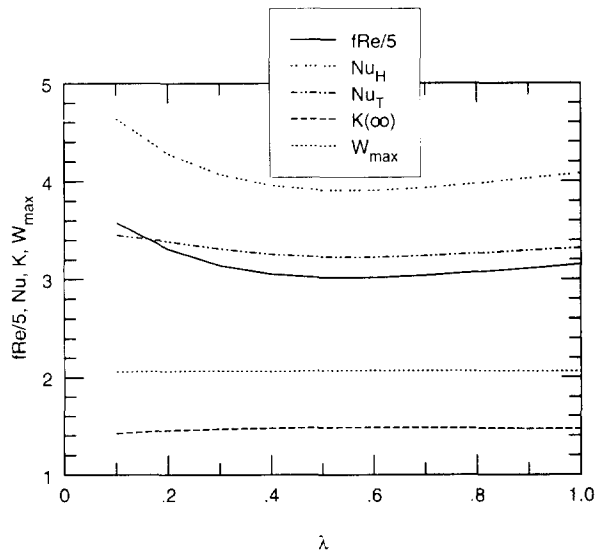

Figure 7 Variation of various quantities with the aspect ratio for ducts with baseplate on the minor axis

duct with those for other ducts, including one value for a parabolic duct. For sinusoidal duct, the values of $f\mathrm{Re}$, Nu_T, and Nu_H decrease monotonically as L/B decreases. However, for semi-elliptic and isosceles triangular ducts, they exhibit a nonmonotonic behavior. While $f\mathrm{Re}$, Nu_T, and Nu_H exhibit a minimum around $L/B = 1$ for the semi-elliptic duct, they all exhibit a maximum around $L/B = 1$ for the isosceles triangular duct. As in the earlier subsection *Comparison with other ducts*, the values of F_T and F_H are higher for the semi-elliptic duct compared to the other ducts. Also, F_T and F_H pass through a maximum around $L/B = 1$ for semi-elliptic and isosceles triangular ducts.

Comparing Tables 3 and 4, it is seen that for both types of semi-elliptic ducts, the value of F_T is around 0.1; whereas, that of F_H is around 0.13, about 30 percent higher.

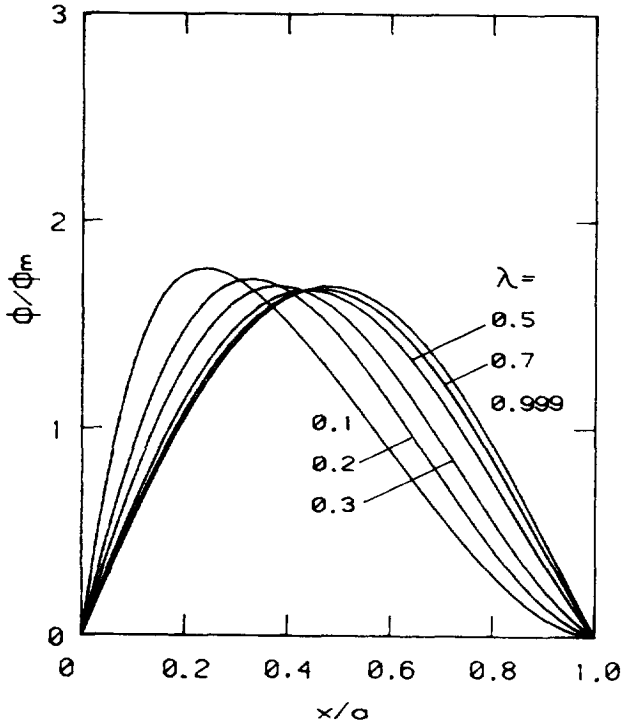

Figure 8 Temperature along the major axis of a duct with baseplate on the minor axis for the Ⓗ boundary condition

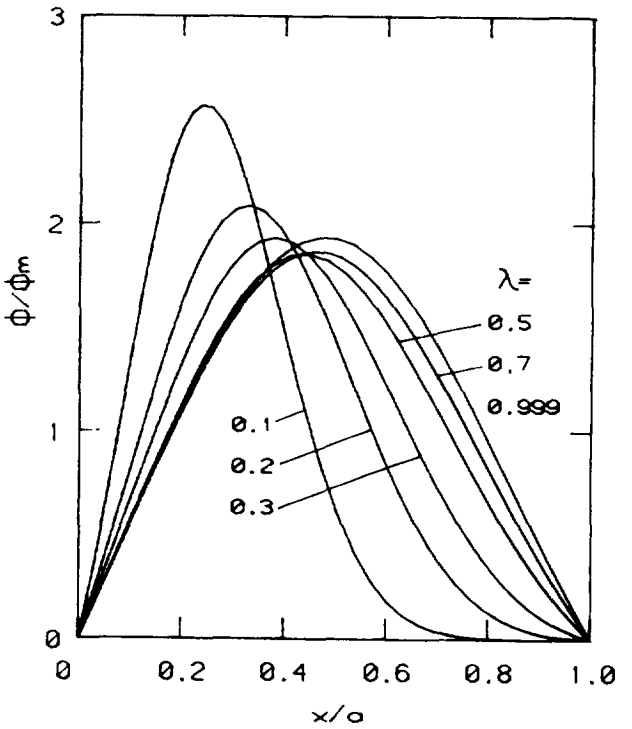

Figure 9 Temperature along the major axis of a duct with baseplate on the minor axis for the Ⓣ boundary condition

Table 4 Comparison of results for semi-elliptic duct with base on the minor axis with those for other ducts

	L/B	λ	Semi-elliptic duct*	Sinusoidal duct†	Isosceles triangular duct†
$2f\mathrm{Re}$	2.0‡	0.25	32.232	29.106	26.052
	1.0	0.5	30.139	26.046	26.642
	0.5	1.0	31.519	22.414	26.306
Nu_T	2.0	0.25	3.348	—	2.22
	1.0	0.5	3.227	2.45	2.46
	0.5	1.0	3.318	2.12	2.34
Nu_H	2.0	0.25	4.175	3.311	2.880
	1.0	0.5	3.910	3.102	3.102
	0.5	1.0	4.080	2.617	2.982
F_T	2.0	0.25	0.1039	—	0.0852
	1.0	0.5	0.1071	0.0941	0.0923
	0.5	1.0	0.1053	0.0946	0.0889
F_H	2.0	0.25	0.1295	0.1138	0.1106
	1.0	0.5	0.1297	0.1191	0.1164
	0.5	1.0	0.1294	0.1168	0.1134

* with base on the minor axis
† Shah and London (1978)
‡ $2f\mathrm{Re} = 30.652$ for a parabolic duct (Shah and Bhatti 1987) for $L/B = 2.0$

Conclusions

A control volume-based discretization method is described for the fully developed laminar flow and heat transfer in semi-elliptical ducts with the baseplate on the major or minor axis. Two types of thermal boundary conditions on the duct wall are analyzed. The following are the main conclusions of the analysis.

For ducts having baseplate on the major axis:

(1) The maximum velocity and pressure defect decrease while the friction factor increases as the aspect ratio decreases.
(2) While Nu_H increases monotonically as the aspect ratio decreases, Nu_T exhibits a maximum at $\lambda = 0.2$.
(3) The friction factor and Nu_H values for $\lambda = 0.1$ are about 25 percent higher than those for the semicircular duct.

For ducts with baseplate on the minor axis:

(1) The location of maximum velocity and temperature move toward the baseplate as λ decreases.
(2) While the maximum velocity and pressure defect exhibit a mild maximum near $\lambda = 0.6$, the friction factor and both Nusselt numbers exhibit a minimum near the same aspect ratio.

For both types of semi-elliptic ducts:

(1) The ratio of Nusselt number to the product of friction factor and Reynolds number is higher for semi-elliptic ducts than that for sinusoidal, circular segmental, and isosceles triangular ducts of the same height-to-base ratio.

Acknowledgments

The first author would like to thank S. B. Bhoje and S. C. Chetal of IGCAR, Kalpakkam for their encouragement and support, and P. Sreenivasan of the IGCAR Computer Centre for the use of computing facilities.

References

Abdel-Wahed, R. M., Attia, A. E. and Hifni, M. A. 1984. Experiments on laminar flow and heat transfer in an elliptical duct. *Int. J. Heat Mass Transfer*, **27**, 2397–2413

Ben-Ali, T. M., Soliman, H. M. and Zariffeh, E. K. 1989. Further results for laminar heat transfer in annular sector and circular sector ducts. *J. Heat Transfer*, **111**, 1089–1093

Bhatti, M. S. 1983. Laminar flow in the entrance region of elliptical ducts. *J. Fluids Eng.*, **105**, 290–296

Bhatti, M. S. 1984. Heat transfer in the fully developed region of elliptical ducts with uniform wall heat flux. *J. Heat Transfer*, **106**, 895–898

Dong, Z. F. and Ebadian, M. A. 1991. Numerical analysis of laminar flow in curved elliptic ducts. *J. Fluids Eng.*, **113**, 555–562

Dong, Z. F. and Ebadian, M. A. 1992a. Effects of buoyancy on laminar flow in curved elliptic ducts. *J. Heat Transfer*, **114**, 936–943

Dong, Z. F. and Ebadian, M. A. 1992b. Convective and radiative heat transfer in the entrance region of an elliptic duct with fins. *Num. Heat Transfer*, **21A**, 91–107

Ebadian, M. A., Topakoglu, H. C. and Arnas, O. A. 1986. On the convective heat transfer in a tube of elliptic cross-section maintained under constant wall temperature. *J. Heat Transfer*, **108**, 33–39

Eckert, E. R. G. et al. 1992. Heat transfer—A review of 1991 literature. *Int. J. Heat Mass Transfer*, **35**, 3153–3235

Garg, V. K. and Velusamy, K. 1989. Developing flow in an elliptical duct. *Int. J. Eng. Fluid Mech.*, **2**, 177–196

Hong, S. W. and Bergles, A. E. 1976. Laminar flow heat transfer in the entrance region of semi-circular tubes with uniform heat flux. *Int. J. Heat Mass Transfer*, **19**, 123–124

Lei, Q. M. and Trupp, A. C. 1989a. Maximum velocity location and pressure drop of fully developed laminar flow in circular sector ducts. *J. Heat Transfer*, **111**, 1085–1087

Lei, Q. M. and Trupp, A. C. 1989b. Further analyses of laminar flow heat transfer in circular sector ducts. *J. Heat Transfer*, **111**, 1088–1089

Lei, Q. M. and Trupp, A. C. 1990. Forced convection of thermally developing laminar flow in circular sector ducts. *Int. J. Heat Mass Transfer*, **33**, 1675–1683

Lundgren, T. S., Sparrow, E. M. and Starr, J. B. 1964. Pressure drop due to the entrance region in ducts of arbitrary cross-section. *J. Basic Eng.*, **86**, 620–626

Manglik, R. M. and Bergles, A. E. 1988. Laminar flow heat transfer in a semi-circular tube with uniform wall temperature. *Int. J. Heat Mass Transfer*, **31**, 625–636

Patankar, S. V. 1980. *Numerical Heat Transfer and Fluid Flow*. Hemisphere/McGraw Hill, Washington

Raithby, G. D. and Schneider, G. E. 1979. Numerical solution of problems in incompressible fluid flow: Treatment of the velocity-pressure coupling. *Num. Heat Transfer*, **2**, 417–440

Shah, R. K. and Bhatti, M. S. 1987. Laminar convective heat transfer in ducts. In *Handbook of Single-Phase Convective Heat Transfer*, S. Kakac, R. K. Shah and W. Aung (eds.). Wiley-Interscience, New York

Shah, R. K. and London, A. L. 1978. *Laminar Flow-Forced Convection in Ducts*. Academic Press, New York

Velusamy, K. 1989. Introduction of whole field solution procedure and porous body formulations in THYC-2D, Internal Note: PFBR/66040/DN/1041/R-A, IGCAR

Velusamy, K. and Garg, V. K. 1993. Entrance flow in elliptical ducts. *Int. J. Num. Meth. Fluids*, **17**, 1079–1096